

# Cavity-mediated coherent coupling between distant quantum dots

Giorgio Nicolí,<sup>1</sup> Michael Sven Ferguson,<sup>2</sup> Clemens Rössler,<sup>3</sup> Alexander Wolfertz,<sup>1</sup> Gianni Blatter,<sup>2</sup> Thomas Ihn,<sup>1</sup> Klaus Ensslin,<sup>1</sup> Christian Reichl,<sup>1</sup> Werner Wegscheider,<sup>1</sup> and Oded Zilberberg<sup>2</sup>

<sup>1</sup>*Solid State Physics Laboratory, ETH Zürich, 8093 Zürich, Switzerland*

<sup>2</sup>*Institute for Theoretical Physics, ETH Zürich, 8093 Zürich, Switzerland*

<sup>3</sup>*Infineon Technologies Austria, Siemensstraße 2, 9500 Villach, Austria*

(Dated: December 25, 2017)

Scalable architectures for quantum information technologies require to selectively couple long-distance qubits while suppressing environmental noise and cross-talk. In semiconductor materials, the coherent coupling of a single spin on a quantum dot to a cavity hosting fermionic modes offers a new solution to this technological challenge. Here, we demonstrate coherent coupling between two spatially separated quantum dots using an electronic cavity design that takes advantage of whispering-gallery modes in a two-dimensional electron gas. The cavity-mediated long-distance coupling effectively minimizes undesirable direct cross-talk between the dots and defines a scalable architecture for all-electronic semiconductor-based quantum information processing.

Quantum information technologies emerge as a promising solution to overcome both the technological and the computational boundaries that limit standard computers [1]. Quantum processing units operate with qubits—quantum bits of information. They are realized using two-levels systems and take advantage of the quantum principles of superposition and entanglement of states [1–3]. These quantum properties can lead to a significant increase in our ability to solve certain types of problems, with notable examples in the fields of cryptography [4] and simulation of quantum many-body systems [5]. Building a quantum computer poses a multitude of challenges as many components need to work together in a robust and scalable fashion. Numerous technologies are currently competing to become the leading platform for quantum information processing [6–8].

Among them, semiconductor materials offer the possibility to encode qubits using artificial atoms embedded in a two-dimensional electron gas—so called quantum dots [9–11]. While single qubit operations via local control have been successfully implemented, two-qubit entanglement requires a tunable coupling that is difficult to achieve. Such coupling should be scalable, noise resistant, and selective, requirements that become increasingly demanding as the density of qubits is increased [6–8, 12]. Dedicated coherent systems that mediate tunable couplings between distant quantum dots offer a potential solution to these challenges. Recently, hybrid superconductor-semiconductor devices have been put forward, demonstrating coherent coupling between a quantum dot and a microwave field confined in a superconducting resonator [13–15]. Conceptually, such large-scale resonators can be used to couple spatially separated qubits.

Such a hybrid solution has to pair different technologies and an all-electronic solution on chip is highly sought after. Examples of the latter include RKKY-mediated coupling between two dots connected by a large open dot [16] and proposals for coupling quantum dots via

edge-modes in the quantum Hall regime [17–19]. An alternative novel approach involves the introduction of an electronic cavity as a mediator of long-distance coupling: recently, such an electronic cavity that sustains coherent fermionic modes [20, 21] has been strongly coupled to a quantum dot [22]. The distinct spin-coherent signatures observed in this dot-cavity setup have spurred further theoretical [1, 23, 25] and experimental [26, 27] work and motivates its use as a quantum bus.

In this work, we demonstrate tunable coherent coupling between distant quantum dots in a mesoscopic semiconducting architecture. Using a novel kind of electronic cavity that sustains whispering-gallery modes [28, 29], we achieve suppression of cross-talk between the dots alongside a selective coupling mechanism. Specifically, we report on four transport spectroscopy experiments that systematically demonstrate these features. Our device can serve as a viable technological solution to the scalability challenge of semiconductor quantum information processors. At the same time, it offers a novel platform for the investigation of fascinating many-body problems in solid state physics such as the two-impurity Kondo system [30].

Our experiments are conducted using different configurations of the device shown in Fig. 1(a). The device is cooled to an electronic temperature of  $\sim 24$  mK in a dilution refrigerator. It is composed of a two-dimensional electron gas that resides 90 nm underneath the surface of a GaAs/AlGaAs heterostructure, where lithographically defined metallic top gates act as Schottky contacts. Applying suitable negative voltages depletes the underlying two-dimensional electron gas to form two spatially separated quantum dots set  $1.7 \mu\text{m}$  apart from each other. Each dot is confined using three finger gates and a large arc-shaped gate (dubbed gallery). In the experiments below, we apply the same fixed voltage  $V_{\text{gallery}}$  to the gallery gate, ensuring depletion of the two-dimensional electron gas and contributing to the electrostatic definition of the dots. The special feature of our device is the

presence of a quasi-1D electronic cavity that sustains coherent whispering-gallery modes, as verified by KWANT simulations [2], see Fig. 1(a). These modes are spin-degenerate states embedded within the Fermi sea, i.e., electron screening effectively removes charging effects on the cavity. Therefore, the cavity modes modulate the local density of states of the central reservoir and couple the two dots. Figure 1(b) shows a schematic energy diagram of the full dot-cavity-dot system with the relevant transport processes between the setup's constituents.

In *experiment I*, we demonstrate the spin-coherent coupling of the electronic cavity and the left dot. The energy of the dot is controlled by the plunger gate voltage  $V_1$ , while the cavity is defined on the left by the dot and on the right by  $V_{B2}$ , which additionally can tune the length of the cavity. We perform equilibrium transport spectroscopy of this system [32] as a function of both  $V_1$  and  $V_{B2}$ , thus tuning the dot and cavity levels while having a small bias-voltage between reservoirs (S) and (R). The result of this experiment is presented in Fig. 1(c), where we observe signatures of a competition between a dot-cavity singlet formation and Kondo transport, similar to Refs. [1, 22]. This result confirms that we have successfully created a coherent fermionic cavity in a novel whispering-gallery mode geometry. Similar experiments confirm the coherent dot-cavity coupling of the second dot.

Having established the existence of an electronic cavity that can couple to our dots, we formulate a simple dot-cavity-dot model for the full device, see Fig. 1(b) [33]. Generally, electrons from each dot can (i) directly tunnel to (R), (ii) tunnel-couple independently to the cavity, forming a dot-cavity hybrid state, or (iii) form a dot-cavity-dot hybrid state with a wavefunction spanning both dots and the cavity, see Fig. 2 for examples of such transport signatures. Tracing out the cavity in case (iii), an effective dot-dot tunnel-coupling is achieved which depends on the energetic configuration of the dot-cavity-dot system. Aligning the cavity-, dot-, and Fermi-levels, the effective coupling is equal to the dot-cavity tunnel amplitude  $t_{\text{eff}} = t_{\text{dot-cav}}$ ; detuning the cavity level by  $\varepsilon_{\text{cav}}$ , a perturbative analysis [33] provides the reduced effective coupling  $t_{\text{eff}} \sim t_{\text{dot-cav}}^2 / \varepsilon_{\text{cav}}$ . Note, that significantly different dot-cavity couplings for the two dots leads to case (ii) and a suppression of  $t_{\text{eff}}$ . We show below that electrostatic interactions between electrons in different dot/cavity elements are negligible.

In *experiment II*, we demonstrate the long-distance coherent coupling between the neighboring dots via the cavity. We study transport through the dot-cavity-dot system as a function of the two plunger gate voltages  $V_1$  and  $V_2$  and in response to a small bias-voltage applied simultaneously to both source (S) and drain (D) reservoirs relative to (R). In Figs. 2(a-c), the currents measured in (S), (R), and (D) are plotted, respectively. In Figs. 2(a) and (c), the measurement of the source ( $I_S$ ) and drain

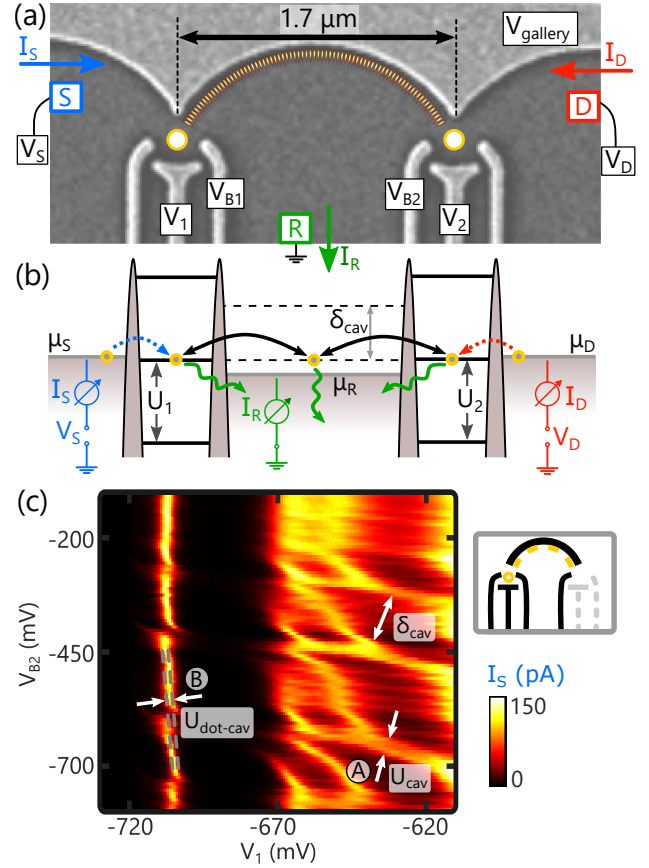


FIG. 1. (a) Scanning electron micrograph of the device; bright features are metallic top-gates. Negative voltages can be applied to all the gates, with labels indicating those explicitly discussed in the text. The (yellow) circles mark the two quantum dots. A numerically calculated local density of states map (using KWANT [2]) of a whispering-gallery cavity mode close to the Fermi energy,  $\varepsilon_F = 7.85$  meV is shown as an overlay. The three boxes (S), (D) and (R) label ohmic contacts to the two-dimensional electron gas. The contact to lead (R) is grounded at all times, while the other two are connected to DC voltage sources. The sign of the measured currents  $I_S$ ,  $I_D$ , and  $I_R$  is positive when electrons flow in the direction of the arrows. (b) Schematic energy diagram of the full dot-cavity-dot system including the confined energy levels of the two dots (black solid lines), the continuous electronic dispersion in the leads (grey boxes), and the cavity modes (black dashed lines). The colored arrows indicate possible transport processes in the system. (c) Transport spectroscopy of the dot-cavity system (experiment I). Vertical lines correspond to transport through resonances of the left dot, while the diagonal lines are identified as cavity modes. Avoided crossings between these two sets of features are evidence of dot-cavity hybridization [1, 22, 23]. The sketch on the right indicates the gates used for this experiment. The width of the cavity levels, indicated by (A) gives an upper bound on the cavity charging energy, while the offset indicated by (B) sets an upper bound on the dot-cavity electrostatic interaction.

currents ( $I_D$ ) allows us to distinguish between the transport across the individual dots. On the other hand, the

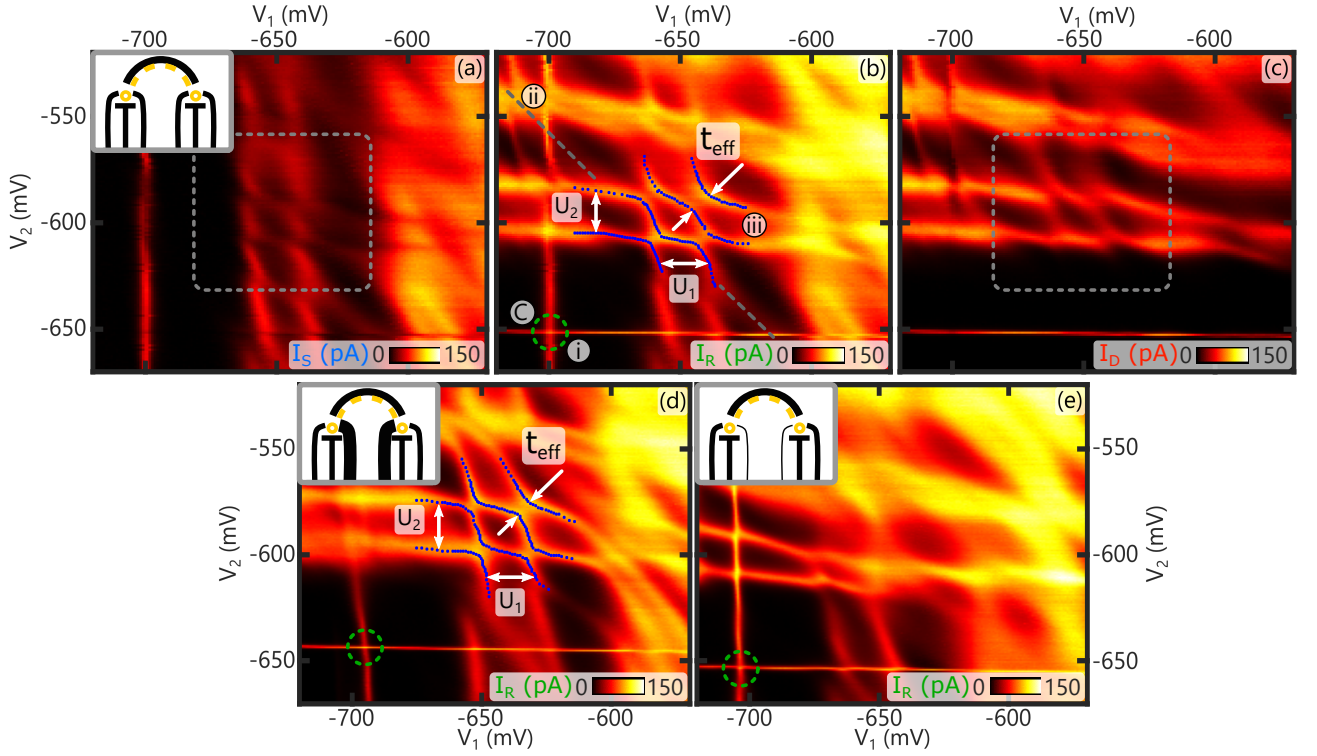


FIG. 2. (a-c) Spectroscopy of the dot-cavity-dot system exhibiting long-distance coupling between the two dots (experiment II, labels are color coded as in Fig. 1). The (grey) boxes in (a) and (c) indicate dot-cavity-dot coupling-related features, corresponding to transport category (iii) (see discussion in the text), i.e., avoided crossings between vertical and horizontal resonances. The charging energy of the two dots  $U_i$  ( $i = 1, 2$ ) is highlighted in (b). The (blue) points correspond to the peak position of the Coulomb resonances. Several avoided crossings appear, one of them indicated by the (white) arrows. The (green) dashed circle in the bottom-left corner belongs to transport category (i) where the two resonances associated with the left and right dot are decoupled [with the individual resonances visible in (a) and (c), respectively]. This crossing constrains the inter-dot charging energy to be negligibly small (C). The dashed (grey) line refers to a transport signature of type (ii). (d,e) Transport measurements of the same system as in experiment II, but with asymmetric tunnel barriers (experiment III). Weaker (d) and stronger (e) coupling regimes of the dot-cavity-dot hybrid are probed [symbols refer to the same quantities as in (b)]. The upper-left insets sketch which gates are active for each measurement.

measurement of the reservoir current  $I_R = I_S + I_D$  in Fig. 2(b) emphasizes the avoided crossings associated with the coherent interdot transport.

The dot-cavity-dot hybrid is modified when changing the plunger gate voltages, giving us access to all three transport categories (i), (ii), and (iii) introduced above. Transport category (i) is clearly seen in the bottom-left corner of Fig. 2(b), where vertical (resp. horizontal) resonance lines meet in a right angle (green dashed circle). Comparing how this feature appears in Figs. 2(a) and (c), we observe that the vertical (resp. horizontal) line results from independent transport through the left (right) dot. Due to the existence of many cavity levels that couple to each of the dots independently, we observe superimposed signatures of transport category (ii), see Figs. 2(a-c) and compare to Fig. 1(c). Diagonal lines in Figs. 2(a-c) [22] are due to coherent coupling of a single dot to the cavity. The grey dashed lines in Fig. 2(b) can be split into left and right transport features by comparing it to the Figs. 2(a) and (c).

The appearance of transport signatures that resemble a double-dot charge stability diagram [34] in all of the three measured currents is clear evidence for the strong coupling between the dots, i.e., for transport category (iii). Most importantly, this coupling is mediated by the electronic cavity as will be further verified in Experiment IV [33]. From the the magnitude of the avoided-crossing gap in Fig. 2(b), we can derive the large dot-dot effective tunnel-coupling  $t_{\text{eff}} \sim 480 \mu\text{eV}$ .

There are three types of electrostatic interaction that potentially contribute to the size of the gaps we have associated to the dot-cavity-dot state, (A) the intracavity charging energy  $U_{\text{cav}}$ , (B) the mutual charging energy  $U_{\text{dot-cav}}$  between the dot and the cavity, and (C) the mutual dot-dot charging energy  $U_{12}$ . For the latter, the clean intersection between dot resonances, see the green dashed circles in Fig. 2(b), limits  $U_{12}$  to a pixel-wide avoided crossing of  $\sim 10 \mu\text{eV}$  [35]. An upper limit for contributions (A) and (B) is obtained by further investigation of Fig. 1(c): the injection of successive electrons

into the cavity only negligibly shifts the Coulomb peaks of the dot, limiting  $U_{\text{dot-cav}}$  to  $\sim 20 \mu\text{eV}$ ; the charging energy of the cavity should be visible as two parallel sets of cavity modes shifted with respect to each other by the Coulomb interaction. We find an upper bound of  $U_{\text{cav}} \simeq 30 \mu\text{eV}$ , given by the finite linewidth of the cavity resonances. All these contributions combined amount to at most  $\sim 10\%$  of the measured coupling energy and we conclude that the gap opening is dominated by coherent tunneling. In summary, we have shown that a coherent dot-dot coupling can be mediated between distant dots using an electronic cavity [36].

It is helpful to place the measured tunnel-coupling  $t_{\text{eff}} \sim 480 \mu\text{eV}$  into context with (other) typical device parameters, e.g., the charging energy of the two dots  $U_1 \simeq U_2 \simeq 1 \text{ meV}$  (highlighted in Fig. 2(b)), the dot single-particle level spacing  $\sim 400 \mu\text{eV}$ , as well as coupling energies obtained in standard double-dot experiments. For the latter, typical tunnel splittings amount to  $\sim 100 \mu\text{eV}$  [37], with the total coupling energy including comparable tunnel and electrostatic contributions [38, 39]. The separation between the dots in the experiments of Refs. [38, 39] is of the order of a few hundred nanometers, while in our sample, the distance between the dots is almost  $2 \mu\text{m}$ . Hence, in spite of the larger separation between dots, the cavity-assisted coupling mechanism studied in the present work provides comparable effective coupling strengths between dots, with the additional advantage of a greatly suppressed electrostatic cross-talk.

In *experiment III*, we report on the gate-tunability of our setup. We establish weak and strong coupling regimes by changing the tunnel barriers (and hence the coupling) of the dots towards the cavity via the voltages  $V_{B1}$  and  $V_{B2}$  [Fig. 1(a)]. In the weak coupling regime [Fig. 2(d)], the barriers confine the dots more strongly, resulting in narrower avoided crossings and a reduced coupling  $t_{\text{eff}} \simeq 330 \mu\text{eV}$ , a  $\sim 31\%$  reduction of with respect to the situation in Fig. 2(b). In the strong coupling configuration [Fig. 2(e)], the reduced confinement of the dots washes out the signatures of strong dot-cavity-dot hybridization that was observed in Fig. 2(c). The coupling between the dots and the cavity increases to the point where we expect the system to behave more like a single quantum dot with a large area, instead of three separated (but coupled) systems. Experiment III offers a path towards achieving complete On/Off switching of the coupling with future improved designs.

In *experiment IV*, we test the potential of the cavity-mediated coupling to extend over longer distances. Taking advantage of a third dot present in our sample [33], we repeat experiment II with a next-nearest-neighbor configuration (see lower inset in Fig. 3). The dots in this case reside  $3.5 \mu\text{m}$  apart from each other and are coupled via a whispering-gallery mode spanning two cavity arcs; the gate controlled by  $V_2$  partially depletes the cen-

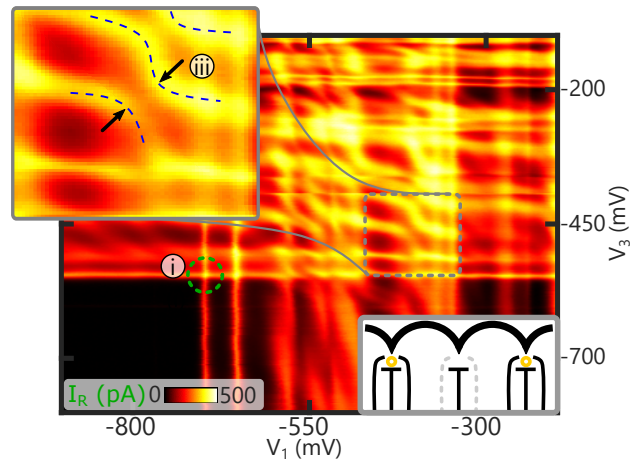


FIG. 3. Transport through a hybrid system consisting of a longer-ranged electronic cavity that couples next-nearest-neighbor quantum dots (experiment IV). The bottom-right inset schematically shows the gates configuration for the experiment [33]. Similarly to experiment II, we find horizontal and vertical type (i) resonances due to separate transport through the energy levels of the two dots. Avoided crossings of type (iii), appear at the intersection between specific resonances, see the magnified upper-left inset (black arrows). These are clear signature for coherent dot-cavity-dot coupling [33]. The (blue) dashed lines are guides to the eye.

tral reservoir without forming a dot and connects the two cavities [33]. In Fig. 3, we observe avoided crossings characteristic of transport category (iii), as highlighted in the upper inset. Along with measurements of the individual source and drain currents [33], we obtain clear evidence of a dot-dot cavity-mediated tunnel coupling. The splitting is observed only when the two-arc gallery mode is formed, i.e., it can be switched using the gate bias  $V_2$  [33].

The long-distance, cavity-mediated tunnel-coupling between dots investigated in our device offers an all-electronic controllable platform for quantum information processing. In particular, the reduced electrostatic cross-talk and the tunable long-distance coherent coupling provide a possible solution to the scalability challenges in semiconducting architectures. Further improvements of our prototypical cavity-design may offer higher-control and selective connectivity, and thus the possibility of entanglement experiments for two or more qubits [40, 41]. Furthermore, our system can be used to study many-body physics phenomena, such as exotic Kondo systems involving two magnetic impurities, i.e., two isolated spins confined in the dots [30], the competition between cavity-assisted and RKKY-mediated coupling [16], as well as, the realization of a potential Kondo-cat state [1].

We thank T. Krähenmann and G. Burkard for illuminating discussions. We acknowledge support from the ETH FIRST laboratory and financial support from the Swiss National Science Foundation, Division 2 and

through the National Centre of Competence in Research "QSIT - Quantum Science and Technology".

- 
- [1] M. A. Nielsen and I. L. Chuang, *Quantum computation and quantum information*, 10th ed. (Cambridge University Press, Cambridge ; New York, 2010).
  - [2] D. Loss and D. P. DiVincenzo, Phys. Rev. A **57**, 120 (1998).
  - [3] J. Clarke and F. K. Wilhelm, Nature **453**, 1031 (2008).
  - [4] P. Shor, SIAM Rev. **41**, 303 (1999).
  - [5] D. S. Abrams and S. Lloyd, Phys. Rev. Lett. **79**, 2586 (1997).
  - [6] M. H. Devoret and R. J. Schoelkopf, Science **339**, 1169 (2013).
  - [7] D. D. Awschalom, L. C. Bassett, A. S. Dzurak, E. L. Hu, and J. R. Petta, Science **339**, 1174 (2013).
  - [8] D. Rotta, F. Sebastiano, E. Charbon, and E. Prati, npj Quantum Information **3**, 26 (2017).
  - [9] T. Hayashi, T. Fujisawa, H. D. Cheong, Y. H. Jeong, and Y. Hirayama, Phys. Rev. Lett. **91**, 226804 (2003).
  - [10] J. Gorman, D. G. Hasko, and D. A. Williams, Phys. Rev. Lett. **95**, 090502 (2005).
  - [11] J. R. Petta, A. C. Johnson, J. M. Taylor, E. A. Laird, A. Yacoby, M. D. Lukin, C. M. Marcus, M. P. Hanson, and A. C. Gossard, Science **309**, 2180 (2005).
  - [12] D. Loss and D. P. DiVincenzo, Phys. Rev. A **57**, 120 (1998).
  - [13] L. E. Bruhat, T. Cubaynes, J. J. Vienne, M. C. Dartailh, M. M. Desjardins, A. Cottet, and T. Kontos, arXiv:1612.05214 [cond-mat] (2016).
  - [14] A. Stockklauser, P. Scarlino, J. V. Koski, S. Gasparinetti, C. K. Andersen, C. Reichl, W. Wegscheider, T. Ihn, K. Ensslin, and A. Wallraff, Phys. Rev. X **7**, 011030 (2017).
  - [15] X. Mi, J. V. Cady, D. M. Zajac, P. W. Deelman, and J. R. Petta, Science **355**, 156 (2017).
  - [16] N. J. Craig, J. M. Taylor, E. A. Lester, C. M. Marcus, M. P. Hanson, and A. C. Gossard, Science **304**, 565 (2004).
  - [17] S.-R. E. Yang, J. Schliemann, and A. H. MacDonald, Phys. Rev. B **66**, 153302 (2002).
  - [18] V. W. Scarola, K. Park, and S. Das Sarma, Phys. Rev. Lett. **91**, 167903 (2003).
  - [19] S. J. Elman, S. D. Bartlett, and A. C. Doherty, Phys. Rev. B **96**, 115407 (2017).
  - [20] J. A. Katine, M. A. Eriksson, A. S. Adourian, R. M. Westervelt, J. D. Edwards, A. Lupu-Sax, E. J. Heller, K. L. Campman, and A. C. Gossard, Phys. Rev. Lett. **79**, 4806 (1997).
  - [21] J. S. Hersch, M. R. Haggerty, and E. J. Heller, Phys. Rev. Lett. **83**, 5342 (1999).
  - [22] C. Rössler, D. Oehri, O. Zilberberg, G. Blatter, M. Karalic, J. Pijnenburg, A. Hofmann, T. Ihn, K. Ensslin, C. Reichl, and W. Wegscheider, Phys. Rev. Lett. **115**, 166603 (2015).
  - [23] M. S. Ferguson, C. Rössler, T. Ihn, K. Ensslin, G. Blatter, and O. Zilberberg, arXiv preprint arXiv:1612.03850 (2016).
  - [1] M. S. Ferguson, D. Oehri, C. Rössler, T. Ihn, K. Ensslin, G. Blatter, and O. Zilberberg, Phys. Rev. B **96**, 235431 (2017).
  - [25] L. G. G. V. Dias da Silva, C. H. Lewenkopf, E. Vernek, G. J. Ferreira, and S. E. Ulloa, Phys. Rev. Lett. **119**, 116801 (2017).
  - [26] C. Yan, S. Kumar, M. Pepper, P. See, I. Farrer, D. Ritchie, J. Griffiths, and G. Jones, Phys. Rev. Applied **8**, 024009 (2017).
  - [27] R. Steinacher, C. Pörtl, T. Krähenmann, A. Hofmann, C. Reichl, W. Zwerger, W. Wegscheider, R. Jalabert, K. Ensslin, D. Weinmann, *et al.*, arXiv preprint arXiv:1709.08559 (2017).
  - [28] C. V. Raman and G. A. Sutherland, Nature (London) **108**, 42 (1921).
  - [29] Y. Zhao, J. Wyrick, F. D. Natterer, J. F. Rodriguez-Nieva, C. Lewandowski, K. Watanabe, T. Taniguchi, L. S. Levitov, N. B. Zhitenev, and J. A. Stroscio, Science **348**, 672 (2015).
  - [30] A. M. Chang and J. C. Chen, Rep. Prog. Phys. **72**, 096501 (2009).
  - [2] C. W. Groth, M. Wimmer, A. R. Akhmerov, and X. Waintal, New J. Phys. **16**, 063065 (2014).
  - [32] C. Rössler, S. Burkhard, T. Krähenmann, M. Rössli, P. Märki, J. Basset, T. Ihn, K. Ensslin, C. Reichl, and W. Wegscheider, Phys. Rev. B **90**, 081302 (2014).
  - [33] See Supplementary Material for more details.
  - [34] W. G. van der Wiel, S. De Franceschi, J. M. Elzerman, T. Fujisawa, S. Tarucha, and L. P. Kouwenhoven, Rev. Mod. Phys. **75**, 1 (2002).
  - [35] T. Ihn, *Semiconductor Nanostructures: Quantum states and electronic transport* (Oxford University Press, 2010).
  - [36] Even though the cavity-mediated strong coupling between dots can be explained both by spinful and spinless models, several indications support the spinful case: the dot-cavity coupling (exp. I) exhibits spin-coherent coupling between a dot and a set of cavity levels with spacing  $\sim 190$   $\mu$ eV; in the double dot case (exp. II) the cavity signatures appear with similar spacing (Fig. 2(a-c)), which suggest that the same set of cavity states is responsible for the coupling observed in experiments I and II.
  - [37] R. H. Blick, D. Pfannkuche, R. J. Haug, K. v. Klitzing, and K. Eberl, Phys. Rev. Lett. **80**, 4032 (1998).
  - [38] T. Hatano, M. Stopa, T. Yamaguchi, T. Ota, K. Yamada, and S. Tarucha, Phys. Rev. Lett. **93**, 066806 (2004).
  - [39] T. Hatano, M. Stopa, and S. Tarucha, Science **309**, 268 (2005).
  - [40] S. Mehl, H. Bluhm, and D. P. DiVincenzo, Phys. Rev. B **90**, 045404 (2014).
  - [41] V. Srinivasa, H. Xu, and J. M. Taylor, Phys. Rev. Lett. **114**, 226803 (2015).



## Supplemental Material for:

### Cavity-mediated coherent coupling between distant quantum dots

Giorgio Nicolí,<sup>1</sup> Michael Sven Ferguson,<sup>2</sup> Clemens Rössler,<sup>1,3</sup> Alexander Wolfertz,<sup>1</sup> Gianni Blatter,<sup>2</sup> Thomas Ihn,<sup>1</sup> Klaus Ensslin,<sup>1</sup> Christian Reichl,<sup>1</sup> Werner Wegscheider,<sup>1</sup> and Oded Zilberberg,<sup>2</sup>

<sup>1</sup>*Solid State Physics Laboratory, ETH Zürich, 8093 Zürich, Switzerland*

<sup>2</sup>*Institute for Theoretical Physics, ETH Zürich, 8093 Zürich, Switzerland*

<sup>3</sup>*Infineon Technologies Austria, Siemensstraße 2, 9500 Villach, Austria*

#### SAMPLE FABRICATION AND DESCRIPTION

Our device was fabricated from a GaAs/AlGaAs modulation-doped, single-interface heterostructure grown by molecular-beam epitaxy (MBE). In this way a two-dimensional electron gas (2DEG) is confined in a triangular potential well in the vertical (growth) direction. The 2DEG is localized in a GaAs layer close to the interface with a GaAlAs layer, and 90 nm below the surface. The sheet electron density of the wafer is  $n_s = 2.2 \times 10^{11} \text{ cm}^{-2}$  and the mobility is  $\mu_e = 3.4 \times 10^6 \text{ cm}^2/(\text{Vs})$ , both measured at 1.3 K with standard magnetotransport techniques.

The base heterostructure was additionally processed to define the desired nanostructures. Using optical lithography, we define ohmic contacts to the electron gas and gate leads. In a final step, we define the finer gate structures using electron-beam lithography. The lithography steps are accompanied by etching or metal evaporation and lift-off processes, and in the case of the ohmic contacts thermal annealing.

An SEM picture of the device is shown in Fig. 1. Five spatially-separated quantum dots can be defined with the metallic top-gates. The dots labeled 1 and 2 are those used for experiments I - III (see main text). The additional dot mentioned in the discussion of experiment IV (main text), is the one labeled 3 in Fig. 1. In the main text, we report on experiments conducted on the labeled dots (1,2 and 3). Similar results were obtained using other dot configurations.

#### ROBUSTNESS OF THE LONG-DISTANCE CAVITY-MEDIATED COHERENT COUPLING

In the main text, the cavity-mediated effective dot-dot coupling extends over a small fraction of the  $V_1, V_2$  phase space. This is a result of the cavity levels being shifted by the change of these voltages. We can significantly increase the phase space fraction by performing linear voltage compensation. The gates which tune the tunnel couplings  $V_{B1}, V_{B2}$  are used to induce an opposite cavity shift to the one caused by the voltages  $V_1, V_2$ . This keeps the cavity levels,  $\epsilon_{c\sigma}$  in the model below, constant throughout a much larger fraction of the  $V_1, V_2$

phase space where we thus observe the dot-dot avoided crossings. This can be seen in Fig. 2, where we performed this experiment in dots 1 and 2.

#### SUPPLEMENTARY DATA FOR EXPERIMENT IV

In experiment IV, we analyze the coupling of next-nearest-neighbor quantum dots (labeled 1 and 3). In this case the cavity spans two arcs of the gallery gate connected by a channel defined by the gate  $V_2$ . Notably, we still observe signatures of coherent dot-cavity-dot hybrid states testifying to the robustness of our setup. In order to properly identify these signatures we consider the source  $I_S$ , drain  $I_D$  and reservoir currents  $I_R = I_S + I_D$  (see Fig. 3). The avoided crossings in  $I_R$  are accompanied by vertical (horizontal) transport features in the source  $I_S$  (drain  $I_D$ ) current. These clearly indicate that changes in one dot are influencing the other and that we have thus set up a coherent hybrid dot-cavity-dot molecule over the double the spatial extent of experiment III.

We found that slightly tuning the channel gate  $V_2 = -500 \text{ mV}$  away from its optimal value is sufficient to switch off the effective dot-dot coupling. The extended cavity is then pinched off into two separate cavities. Additionally, we can turn off the effective coupling by grounding  $V_2$  such that the cavity is no longer well defined. The latter case can be seen in Fig. 4, where we observe only the superposition between two sets of horizontal (vertical) resonant lines corresponding to an extended region of transport category (i).

#### THEORETICAL MODEL

We follow the methods laid out in Ref. [S1] to obtain an effective model describing the dot-cavity-dot device. We first simulate the single particle properties of the cavity using KWANT [S2], we then argue for the removal of Fano interference terms based on the two dimensionality of the system and thus arrive at a model which can be represented pictorially, as in Fig.5.

This model Hamiltonian reads

$$H = H_{\text{molecule}} + H_{\text{leads}} + H_{\text{coupling}}, \quad (\text{S1})$$

where the molecular Hamiltonian,

$$H_{\text{molecule}} = H_{\text{dots}} + H_{\text{cav}} + H_{\text{tun}}, \quad (\text{S2})$$

describes the dot-cavity-dot system. It is in turn split into a dot contribution

$$H_{\text{dots}} = \sum_{\alpha, i, \sigma} \epsilon_{\alpha i \sigma} d_{\alpha i \sigma}^\dagger d_{\alpha i \sigma} + \sum_{\alpha} U_{\alpha} \frac{n_{\alpha}^2 - n_{\alpha}}{2}, \quad (\text{S3})$$

where  $\alpha = 1, 2$  indexes the two different dots,  $i \in \mathbb{N}$  indexes the states in the given dot, and  $\sigma = \uparrow, \downarrow$  indexes the spin. The energy  $\epsilon_{\alpha i \sigma}$  gives the energy of the corresponding,  $\alpha, i, \sigma$  state while  $U$  is the interaction energy of the dots (taken to be equal in each dot). Additionally we have introduced the fermionic creation and annihilation operators  $d_{\alpha i \sigma}^\dagger, d_{\alpha i \sigma}$  corresponding to the state  $\alpha, i, \sigma$ , and the total number of particles in a given dot is

$$n_{\alpha} = \sum_{i, \sigma} d_{\alpha i \sigma}^\dagger d_{\alpha i \sigma}. \quad (\text{S4})$$

The cavity is assumed to be a set of energetically equidistant non-interacting fermionic levels and are thus described by

$$H_{\text{cav}} = \sum_{n, \sigma} (\epsilon_{c\sigma} + n\delta_c) c_{n\sigma}^\dagger c_{n\sigma}, \quad (\text{S5})$$

where  $n = 0, \pm 1, \pm 2, \dots$ , up to a cutoff where the equidistant approximation is no longer valid. We have also introduced the cavity level spacing  $\delta_c$ , the energy of the zeroth cavity level  $\epsilon_{c, \sigma}$  and the cavity creation and annihilation operators  $c_{n\sigma}^\dagger, c_{n\sigma}$ . The final piece of the artificial molecule Hamiltonian is the tunneling term between the two dots and the cavity

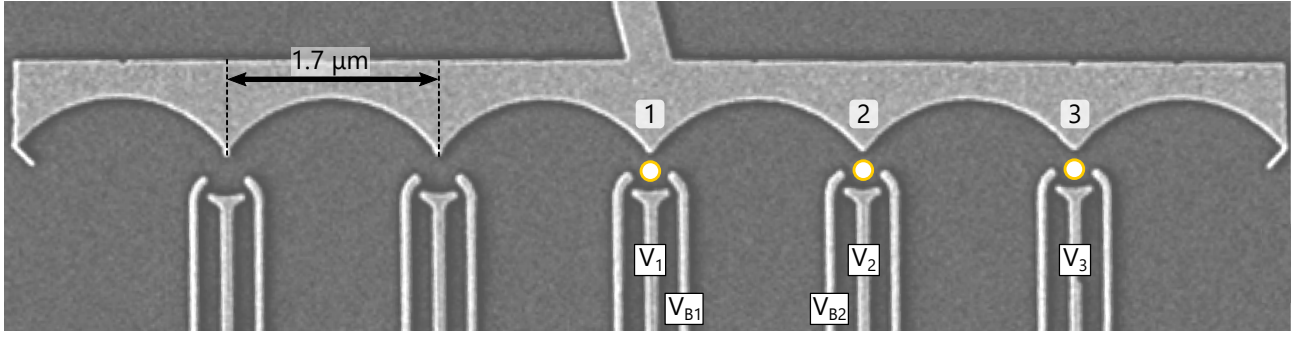
$$H_{\text{tun}} = \sum_{\alpha, i, n, \sigma} \Omega_{\alpha} d_{\alpha, i, \sigma}^\dagger c_{n, \sigma} + h.c., \quad (\text{S6})$$

where  $h.c.$  stands for Hermitian conjugate and the tunneling amplitude  $\Omega_{\alpha}$  is a function of which dot  $\alpha$  the tunneling involves only.

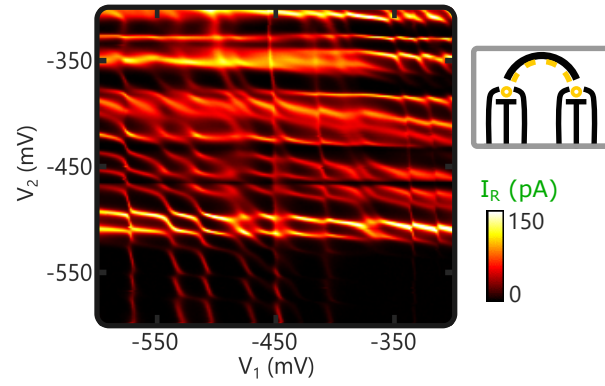
The  $H_{\text{leads}}$  and  $H_{\text{coupling}}$  terms describe three leads coupled directly to either the dots or the cavity with energy independent tunneling amplitudes. For the purpose of calculating the ground state of the molecular Hamiltonian they are unimportant as they serve only to provide a chemical potential  $\mu \equiv 0$  which we define as the zero point of energy.

As there is no magnetic field in the experiment we immediately have  $\epsilon_{\alpha i \sigma} \equiv \epsilon_{\alpha i}$  and  $\epsilon_{c\sigma} \equiv \epsilon_c$ . For simplicity we restrict ourselves to the case of a single state in each dot  $\epsilon_{\alpha, i, \sigma} \equiv \epsilon_{\alpha}$  and the cavity  $\delta_c \rightarrow \infty$  such that there are only 64 states in the Hilbert space which can be easily diagonalized numerically to find good agreement with the experiment. The bottom-left to top-right diagonal in Fig. 2 of the main text, along which the avoided crossings associated with coherent coupling of the two dots occur corresponds to the case  $\epsilon_1 = \epsilon_2$ . This case can be treated analytically to extract the gap sizes. Writing down the Hamiltonians in their matrix representation following [S1], we immediately find that there are two principal regimes: when the cavity level is resonant with the Fermi energy  $\epsilon_c = 0$  we obtain a gap  $\sim \Omega$  (as in degenerate perturbation theory); on the other hand when the cavity is far detuned we obtain a gap  $\sim \Omega^2/\epsilon_c$  (as in non-degenerate perturbation theory). A future experiment with a direct handle on the cavity level will be able to explore these scalings.

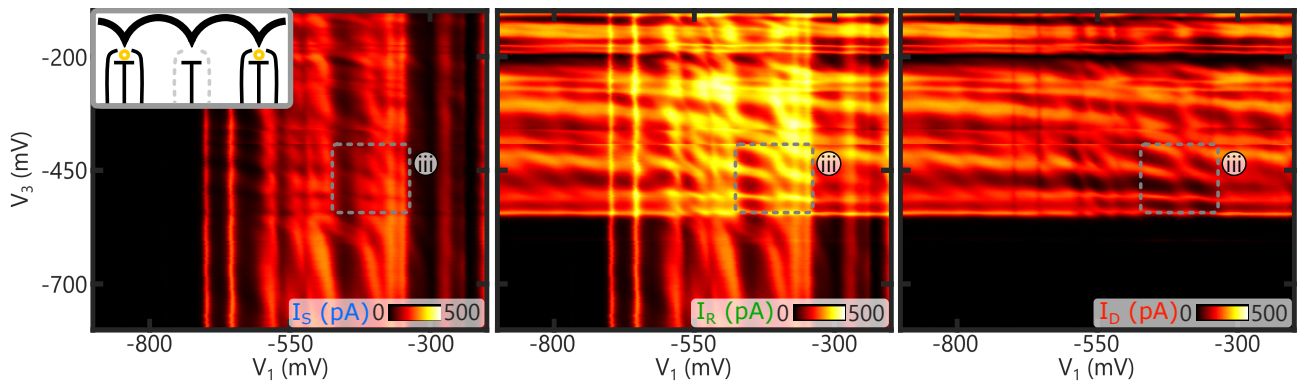
- 
- [S1] M. S. Ferguson, D. Oehri, C. Rössler, T. Ihn, K. Ensslin, G. Blatter, and O. Zilberberg, arXiv:1705.11145 [cond-mat] (2017).  
[S2] C. W. Groth, M. Wimmer, A. R. Akhmerov, and X. Waintal, New J. Phys. **16**, 063065 (2014).



Supplementary Information Figure 1. Scanning electron micrograph of our device. The picture shows the part of the sample with metallic top gates defined by electron-beam lithography. Gate leads and ohmic contacts defined with optical lithography are outside the scanned area.

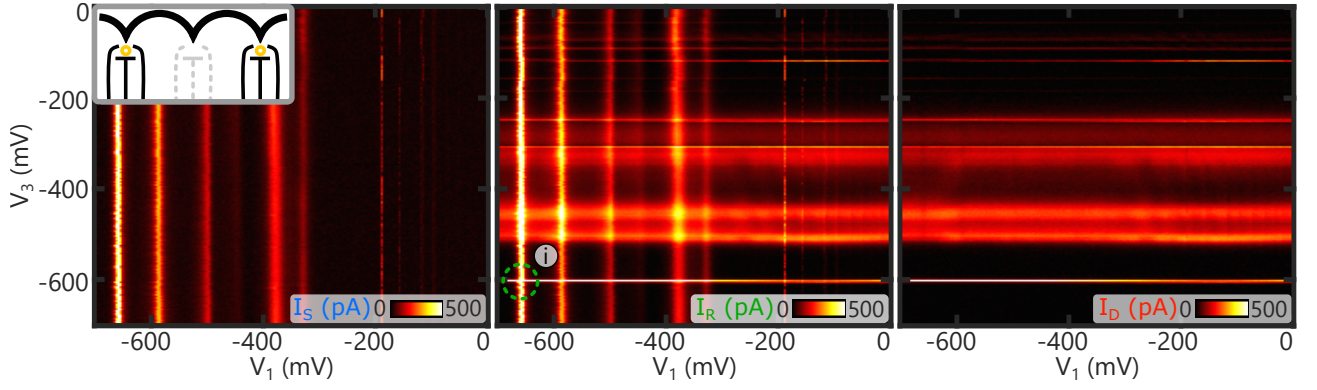


Supplementary Information Figure 2. Equilibrium transport spectroscopy of neighboring coupled quantum dots (dots 1 and 2). Vertical and horizontal lines correspond to transport through the Coulomb resonances of left and right dot, respectively. Multiple avoided crossings between the two sets of resonances are observed, which are signatures of a dot-cavity-dot hybrid. The cavity levels are kept at constant energies by compensating the  $V_1, V_2$  induced shift by an equal and inverse  $V_{B1}, V_{B2}$  shift such that the avoided crossings are observed over a large fraction of the phase-space. The sketch on the right indicates the gates biased for this experiment.

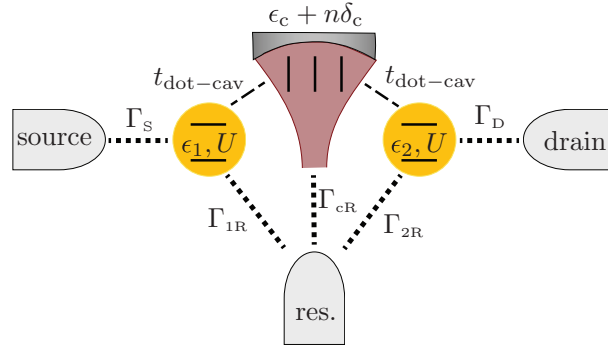


Supplementary Information Figure 3. Spectroscopy of the next-nearest-neighbor quantum dots system (experiment IV, dot 1 and 3). In the grey dashed box, we identify signatures of coherent transport across the entire device [transport category (iii)]. Namely the avoided crossings in  $I_R$  are accompanied by vertical (horizontal) transport features in the source  $I_S$  (drain  $I_D$ ) current and thus corresponds to the formation of a dot-cavity-dot hybrid.





Supplementary Information Figure 4. Spectroscopy of the next-nearest-neighbor quantum dots system (experiment IV, dot 1 and 3) with gate  $V_2$  grounded. In this case, only transport category (i) is observed. The green dashed circle highlights one of the many clean intersection between the sets of vertical and horizontal resonant lines. These features correspond to electron tunneling through unperturbed dots' resonances, identifiable by comparing the measurement of source ( $I_S$ ) and drain ( $I_D$ ) currents (left and right panels, respectively).



Supplementary Information Figure 5. A pictorial representation of the effective model. It includes three leads (source, drain, and reservoir), two dots with independent levels  $\epsilon_1, \epsilon_2$ , equal onsite interaction  $U$ , and a cavity with levels spaced at  $\epsilon_c + n\delta_c$ , where  $n$  is an integer. The rates  $\Gamma$  (dotted lines) weakly couple the dot-cavity-dot molecule to the leads and provide a chemical potential  $\mu$ , while  $t_{\text{dot-cav}}$  coherently couples the dots to the cavity. Note that the three couplings to the reservoir must be accounted for in such a way as to avoid an artificial Fano interference term [S1].